



3D printing of soft thermoplastic elastomers: Effect of the deposit angle on mechanical and thermo-mechanical properties

Adel Tayeb, Jean-Benoit Le Cam, Bruno Loez

► To cite this version:

Adel Tayeb, Jean-Benoit Le Cam, Bruno Loez. 3D printing of soft thermoplastic elastomers: Effect of the deposit angle on mechanical and thermo-mechanical properties. *Mechanics of Materials*, 2022, 165, pp.104155. 10.1016/j.mechmat.2021.104155 . hal-03448149

HAL Id: hal-03448149

<https://hal.science/hal-03448149>

Submitted on 7 Jan 2022

HAL is a multi-disciplinary open access archive for the deposit and dissemination of scientific research documents, whether they are published or not. The documents may come from teaching and research institutions in France or abroad, or from public or private research centers.

L'archive ouverte pluridisciplinaire **HAL**, est destinée au dépôt et à la diffusion de documents scientifiques de niveau recherche, publiés ou non, émanant des établissements d'enseignement et de recherche français ou étrangers, des laboratoires publics ou privés.



Distributed under a Creative Commons Attribution - NonCommercial 4.0 International License

- Specimens of soft TPE-S were printed by Fused Deposition Modelling
- Three different deposit angles were considered
- Thermo-mechanical properties were characterized
- The printing strategy has not a significant effect on the mechanical response
- It has a more significant effect on the thermal response, especially the self-heating.

3D printing of soft thermoplastic elastomers: effect of the deposit angle on mechanical and thermo-mechanical properties

Adel Tayeb^a, Jean Benoit Le Cam^a, Bruno Loez^b

^a *Université de Rennes 1, Institut de Physique UMR 6251 CNRS/Université de Rennes 1, Campus de Beaulieu, Bat. 10B, 35042 Rennes Cedex, France.*

^b *Cooper Standard, 36, rue Pierre et Marie Curie, 35500 Vitré, France.*

Abstract

This work presents the first experimental characterization of the mechanical and thermomechanical properties of a soft 3D printed thermoplastic styrenic elastomer. The tested specimens were obtained by Fused Deposition Modeling with a modified commercial 3D printer. Three different deposit strategies (deposit angle of 0° , 45° and $\pm 45^\circ$) have been tested. Scanning electronic Microscopy was used for analyzing the microstructure of the printed specimens. The specimens were tested under two different uniaxial tensile loadings. The first one consists in applying several sets of load-unload cycles at three increasing strain levels. The second one corresponds to one load-unload cycle at different loading rates. For both tests, the temperature variations were characterized by means of infrared thermography. Results showed that the printing strategy does not have a significant effect on the mechanical response, including the softening, the hysteresis loop and the permanent set, but has an effect on its thermal response. Differences found in terms of self-heating **due to intrinsic dissipation** clearly show that the deposit angle influences the viscosity of the specimens.

Key words: 3D printed TPE, thermomechanical characterization, self-heating, Infrared thermography

1. Introduction

Thanks to their thermomechanical properties and ease of processing, flexible parts made of thermoplastic elastomers **TPE** are omnipresent and are used in almost all industrial sectors, among these are consumer products (seals for food packaging, ergonomic parts of toothbrushes, toys), construction and industry (tool handles, window profiles, junction boxes), medical (pharmaceutical pack-
 5 aging, masks, cannulas) or the automobile industry, typically for sealing. These materials are traditionally manufactured through an injection process requiring

Email address: Jean-benoit.lecam@univ-rennes1.fr (Jean Benoit Le Cam)

the use of a mould. This mould generally needs several iterations of prototyping (2 to 4 in average) to converge towards the final mould/part pair, and remains an important part of the industrialization cost (it can reach several 100 k€ for one prototype mould). In this context, additive manufacturing (AM) is a very promising lever to limit prototyping costs and has shown a concrete interest in making prototype parts and small series. From a historical point of view, AM started in the 1980's by the rapid prototyping, in order to improve and validate the designs before the manufacturing phase. Many AM technologies have been developed since, namely stereolithography (SL) [1], Polyjet [2], fused deposition modeling (FDM) [3], laminated object manufacturing (LOM) [4], 3D printing (3DP), Prometal, selective laser sintering (SLS) [5], laminated engineered net shaping (LENS) [6] and electron beam melting (EBM) [7] among others, see [8], [9], [10] and [11] and references therein for an overview of AM technologies. Since, AM technology has been increasingly employed not only in prototyping cycle but also in the volume production phase for a large industrial fields, such as automotive [12], aerospace [13] and medicine [14], [15]. Today, several materials can be used in AM technologies, going from polymers [16], [17], [18] and ceramics [19], [20], [21] to metallic materials [22], [23]. However, although relatively mature on metallic materials or other branches of plastics processing (PLA, Polyamides, ABS, etc.), the AM technology is at a very early stage of maturity on flexible elastomer materials with the FDM technology, especially the printing of soft parts. To go further, it will be necessary to develop or to extend 3D printable polymer material families, especially TPE-S (or TPS). Indeed, their hardness can be as low as 50/60 shore A, which leads to very soft parts.

This is the reason why a specific head to be connected to a commercial 3D printer has recently been developed in our research group and parts made of soft TPE-S are now 3D printed with a A4v4 model supplied by the 3ntr company. This study presents the mechanical and thermomechanical properties of such a printed material and highlights the effects of the printing strategy, especially the deposit angle considered, on these properties.

The paper is organized as follows: Section 1 presents the experiments: the 3D printing device, the material and specimens geometry, as well as the experimental characterization carried out. Section 3 presents the temperature measurements. The results obtained are reported and discussed in section 4. Concluding remarks close the paper.

2. Experiments

2.1. 3D printing device

The 3D printer is a A4v4 model supplied by the 3ntr company, a provider of additive manufacturing systems (see Figure 1). The manufacturing technology considered here is the FDM. This printer offers a large range of values for the main printing parameters:

- maximal nozzle temperature of 450°C.

- four nozzle diameters: 0.3, 0.4, 0.6 and 0.8 mm .
- maximum printing table temperature of $160^{\circ}C$.
- maximum temperature of the printing zone of $90^{\circ}C$.
- three different materials can be extruded at the same time.
- maximum printing volume $295 \times 195 \times 190 \text{ mm}^3$.



Figure 1: The 3ntr 3D printer (A4v4 model)

In its commercialized configuration, the printer enables us to print TPE parts of a certain stiffness, but not as softer as needed for applications such as automotive sealing systems. In order to make possible the printing of softer TPE, the Cooper Standard company has recently re-designed the printing head to improve the performances in terms of thrust power: the engine has been moved over the machine, which significantly improves the regularity of the engine speed and avoids any micro-dispersion in the extruded volume. Further information is not provided due to confidentiality aspects, neither picture of the modified printer.

2.2. Material, specimen geometry and printing configurations

The material is a thermoplastic styrenic elastomer (TPS or TPE-S). It contains two types of copolymer: polystyrene polybutadiene polystyrene (SBS) and

polystyrene poly(ethylene-butylene) polystyrene (SEBS). Wires of $2.85 \pm mm$ in diameter were first made with a home-made spinning machine and then used in the printing device. The glassy temperature of the material is $-55^\circ C$. The specimen geometry is given in Figure 2a. It is a $105 mm$ long, $30 mm$ width and $2 mm$ thick tensile specimen equipped with cylindrical ends with a diameter of $10 mm$ to avoid any slippage in the machine grips. These specimens were obtained with the printing machine described above. Three printing configurations for the layers depositing were studied, depending on the deposit angle with respect to the tensile loading direction (along the specimen length): 0° , 45° and $\pm 45^\circ$. These three configurations are depicted in Figure 2b. An illustration of the printing process is given in Figure 3. It is shown the printing for 2 configurations, 0° and 45° . For the latter, the first layer deposition is shown at the top right corner of Figure 3. The schematic view at the bottom introduces the terminology that will be used in the following for denoting the specimen surfaces.

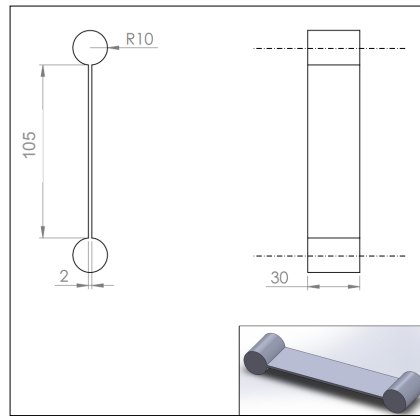
The filament diameter was set at $0.4 mm$. The temperature of the deposit filament is at $230^\circ C$ at the nozzle outlet. This temperature is much greater than the melting temperature of the material. Except the angle chosen, the other deposit parameters were the same: the nozzle diameter was $0.4 mm$, in a layer, the distance between two deposit paths was $0.4 mm$. The nozzle temperature and the thrust power made a cross-section geometry more and more close to a rectangle of $0.4 \times 0.15 mm^2$, as illustrated in Figure 4. Therefore, one of the qualitative criterion for optimizing the printing parameters was the minimization of the void between four filaments of two successive layers (see the bowed zone in dotted line in the figure).

The microstructure of the printed specimens was analyzed with scanning electron microscope (SEM). To this end, secondary electron images of the specimen surface were recorded with a JSM JEOL 7100 F SEM. For each configuration, the specimens were cut with a razor-blade perpendicularly to the loading direction. SEM images of the specimen slices are reported in Figures 5, 6 and 7 for the 0° , 45° and $\pm 45^\circ$ configurations, respectively.

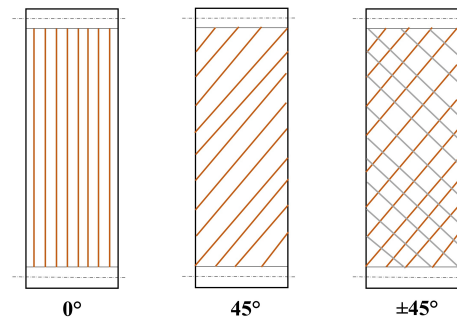
In the case of the 0° and 45° configurations, voids located in the junction area between filaments were observed. From them, the mean distance between the filaments and the mean layer thickness can be determined. They were found to be equal to about $400 \mu m$ and $150 \mu m$, respectively, which is in good agreement with the deposit strategy illustrated in Figure 4. For the $\pm 45^\circ$ configuration, Figure 7 shows that only a few voids were revealed when cutting the specimen, not enough for distinguishing the filaments. Therefore, changing the orientation of the filaments from one layer to the other one decreases the residual voids between filaments and increases the specimen's homogeneity.

2.3. Loading conditions

The experimental setup is shown in Figure 8. It consists in a biaxial tensile machine composed of four independent electrical actuators controlled by an in-house LabVIEW program. Two load cells, whose capacity is equal to $1000 N$, store the force in the two perpendicular directions. In the present study, only



(a) Specimen geometry



(b) printing configurations

Figure 2: Specimen geometry (dimensions in mm) and printing configurations

the vertical axis of the machine was used to apply the uniaxial tensile loadings.

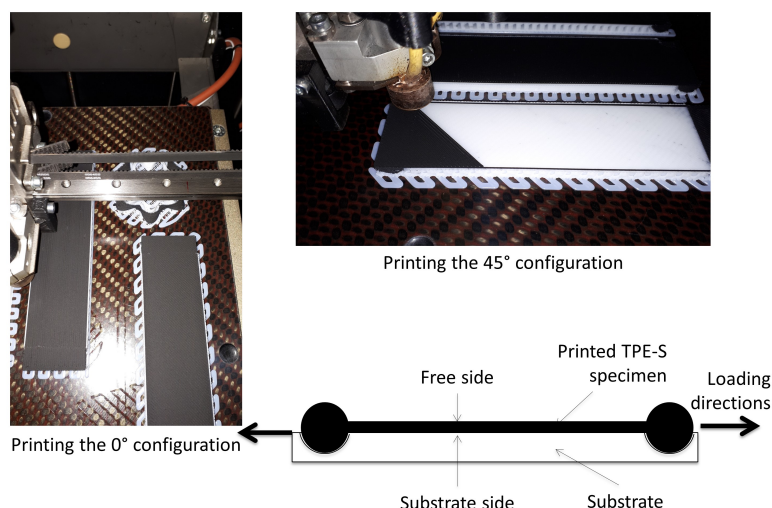


Figure 3: Overview of the printing result

115 An infrared camera was placed on the side of the testing machine and measured the temperature in the specimen surface plane. It should be noted that the loading is symmetrical, meaning that the central zone of the specimen, where the thermal measurement was carried out, did not move.

120 The specimens previously presented were subjected to two different mechanical tests. The first test consisted in applying 5 cycles of loading-unloading (in the vertical direction) on the specimens at three increasing stretch levels of 1.43, 1.87 and 2.33. The prescribed displacement for this test is reported in Figure 9a. The aim of this test was to assess the mechanical behavior of the material with respect to the permanent set and the accommodation. The second one consisted in prescribing a displacement of 165 mm per actuator with two different displacement rates of 50 mm/min and 500 mm/min, respectively. 125 The value of the prescribed displacement was the maximum allowed with the current equipment, i.e. 165 mm per branch. The prescribed displacements for the two displacements rates are shown in Figure 9b.

130 3. Temperature measurement

Temperature measurement was performed with a FLIR X6540sc InSb infrared camera (640 × 512 pixels, wavelength ranges between 1.5 and 5.1 μm,

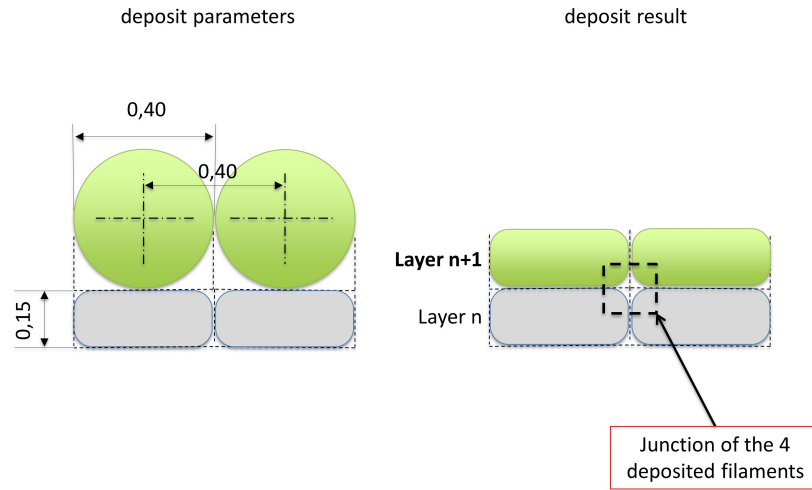


Figure 4: Illustration of the deposit process in the case of the 0° configuration (dimensions in mm)

detector pitch of $15 \mu\text{m}$). The acquisition frequency was set at 5 Hz . The thermal resolution, namely the noise-equivalent temperature difference (NETD), was equal to 20 mK at 25°C . The calibration of camera detectors was performed with a black body using a one-point Non-Uniformity Correction (NUC) procedure at this acquisition frequency. Temperature measurement was performed at the specimen centre, by averaging the temperature in a small zone of 5×5 pixels at the centre of the specimen. Temperature variation is obtained by subtracting the initial averaged temperature to the current one.

4. Results and discussion

In this section, the mechanical response of the specimens for the two mechanical tests is first presented and analyzed in terms of the nominal stress, defined as the ratio of the actual force by the reference cross section, versus the stretch response. The temperature variation over the motionless part of the specimen is then given and discussed.

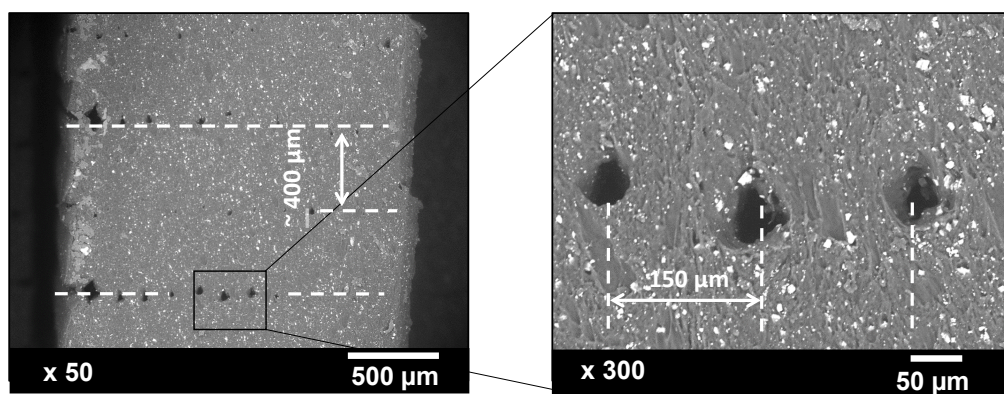


Figure 5: SEM images of the 0° configuration

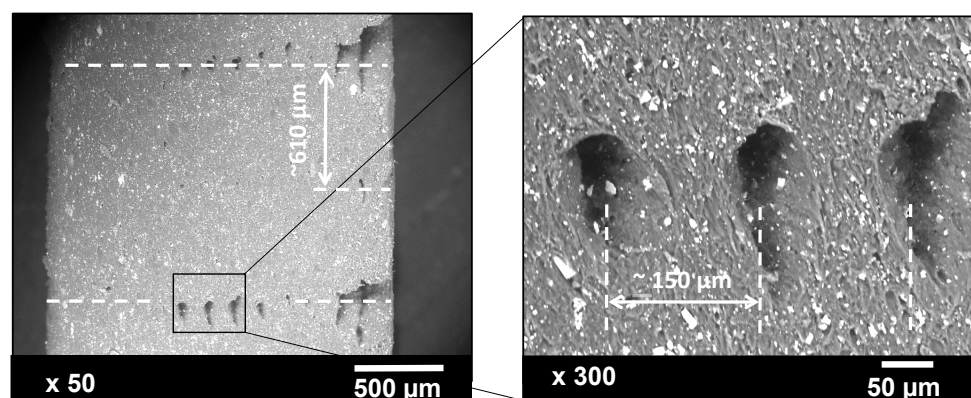


Figure 6: SEM images of the 45° configuration. Here, the voids are elliptical, the filaments are oriented at 45° with respect to the cutting plane.

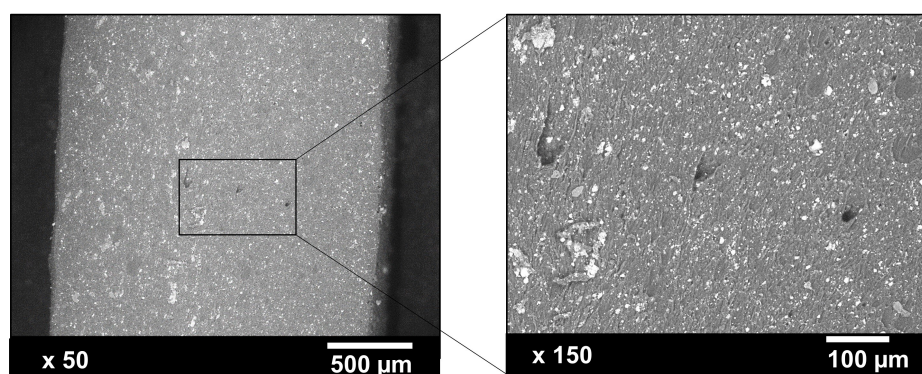


Figure 7: SEM images of the $\pm 45^\circ$ configuration

4.1. Mechanical response

The nominal stress-stretch curves obtained from the first test, corresponding to the cyclic mechanical loading, are reported in Figure 10. For each printing configuration, 3 specimens were tested. This figure highlights that the tests were repeatable, since the response of the three specimens from each configuration are very close. Figure 11 provides the mean nominal stress obtained for each configuration versus stretch. It appears that the nominal stress is slightly different from one configuration to another. In fact, even though all configurations have the same nominal stress response up to an applied strain of 5% (stretch of 1.05), the responses of the three configurations slightly differ above this stretch. The 0° configuration is the stiffest and the $\pm 45^\circ$ configuration is stiffer than the 45° one. Therefore, it can be assumed that the microstructure deformation is influenced by the printing strategy. This idea can be supported by SEM observations performed at the surface of virgin specimens. The SEM images that are presented in Figure 12 clearly highlight the deposit angle, which confirms that the microstructure is initially oriented. Thus, contrarily to the 0° configuration, the microstructure of the 45° and $\pm 45^\circ$ configurations can slightly reorient to adapt the uniaxial tension. This is not the case for the 0° configuration for which the microstructure is oriented in the tensile direction. This reorientation effect is illustrated in Figure 13.

The stress-stretch responses of the three configurations exhibited the same strong non-linearities typically observed in filled elastomers or thermoplastic urethane [24], namely the stress softening (also called the Mullins effect [25]), hysteresis and residual strain. The Mullins effect is a characteristic of filled rub-

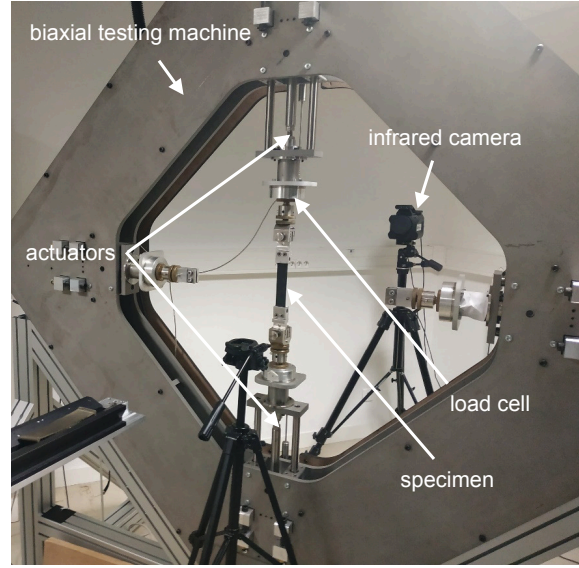
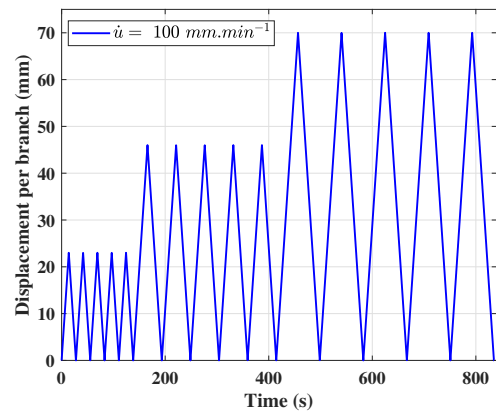


Figure 8: Experimental setup

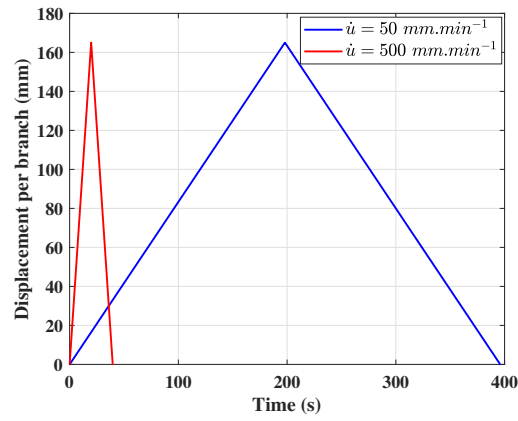
bers emerging as the dependence of the stress-strain curves upon maximum loading previously encountered. It is considered as a damage phenomenon [26], [27] or macromolecular network alteration by the modeling approaches [28]. In the work by [29] aiming to characterize and model the Mullins effect in silicone filled rubber, this phenomenon was quantified by using the ratio between the mechanical energy brought to the specimen during the second loading W_{2l} and the first loading W_{1l} . The mechanical energy is given by

$$W_{il} = \int_1^{\lambda_{\max}} \pi d\lambda, \quad i = 1, 2, \quad (1)$$

where π is the nominal stress in the loading direction and λ_{\max} is the maximal stretch for the studied loading cycle. In a recent work [24], this calculation of the softening has been readapted in order to account for the loading history as

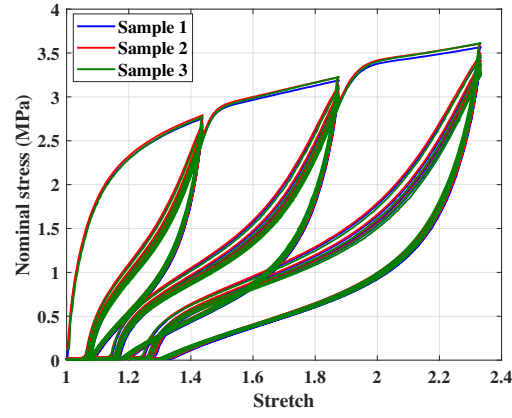


(a) Prescribed displacement in each branch for the first test

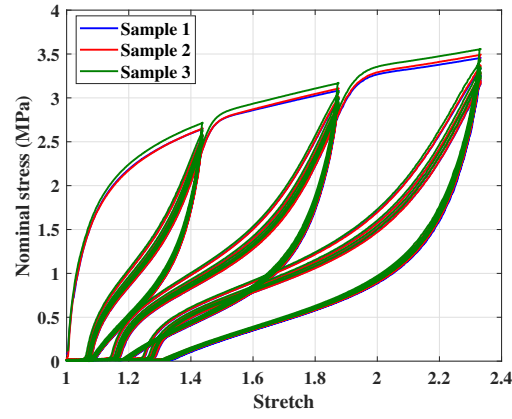


(b) Prescribed displacement in each branch for the second test

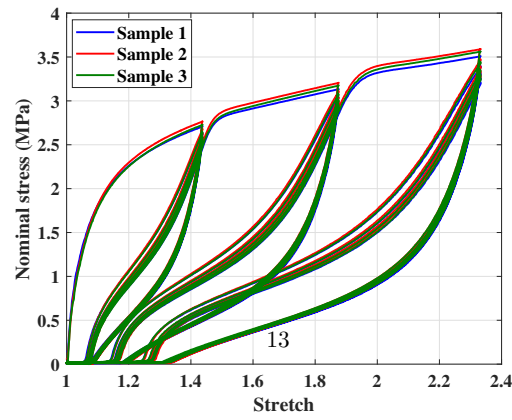
Figure 9: Prescribed displacement for the two experiments



(a) 0° configuration



(b) 45° configuration



(c) ±45° configuration

Figure 10: Nominal stress vs stretch

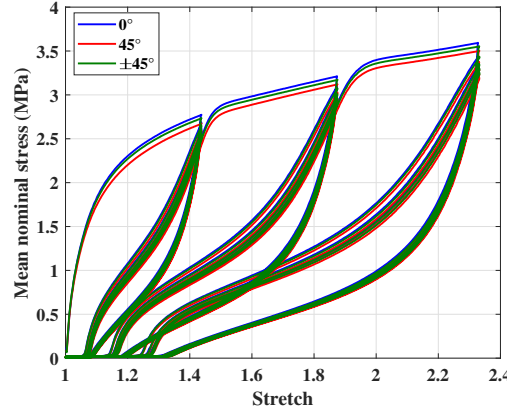


Figure 11: Mean nominal stress vs stretch for the three configurations

if the material has not been subjected to mechanical cycles at lower maximum stretches. The energy brought to the material during the first loading is recalculated and is denoted by W_{1l}^* . It is calculated as explained in Figure 14. The softening ratio is then obtained by dividing the energy brought to the material in the second loading W_{2l} by this energy W_{1l}^* . Figure 15 shows this ratio for the three printing strategies. No significant difference is observed between the different configurations: the accommodation level decreases from around 55% to 41% with increasing maximum principal stretch applied.

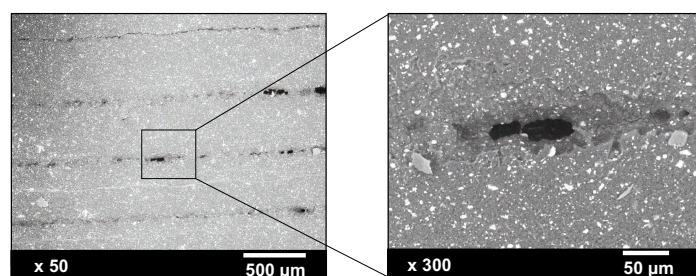
Another phenomenon observed is the hysteresis, which corresponds to the area between the loading and the unloading once the behavior of the specimen is stabilized. It is measured by the following equation:

$$W_5 = W_{5l} + W_{5u} = \int_1^{\lambda_{\max}} \pi d\lambda + \int_{\lambda_{\max}}^1 \pi d\lambda, \quad (2)$$

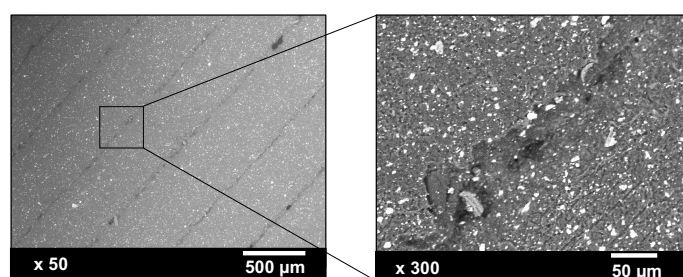
where the subscripts $5l$ and $5u$ refer to the fifth loading and unloading, respectively. In order to take into account the stretch level in its computation, this hysteresis is divided by the energy brought to the specimen during the fifth loading W_{5l} as follows:

$$\frac{W_{5l} + W_{5u}}{W_{5l}}. \quad (3)$$

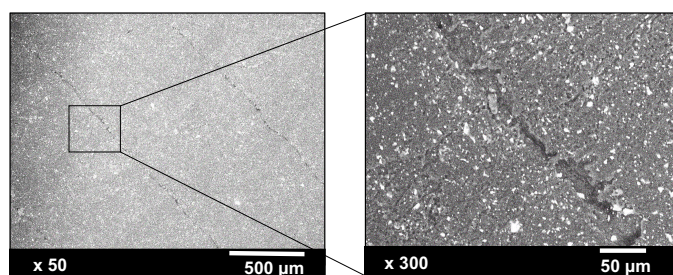
Figure 16 shows this relative hysteresis calculated for the three configurations. The hysteresis is decreasing non linearly with an increasing maximum stretch applied. It lays between 31% and 38% from the energy brought to the specimen during the fifth loading W_{5l} . It should be noted also that the hysteresis is quite similar between the 45° and $\pm 45^\circ$ configurations with a slight difference to the 0° configuration's one.



(a) 0° configuration



(b) 45° configuration



(c) $\pm 45^\circ$ configuration

Figure 12: SEM images of the virgin specimen surface highlighting the deposit angle

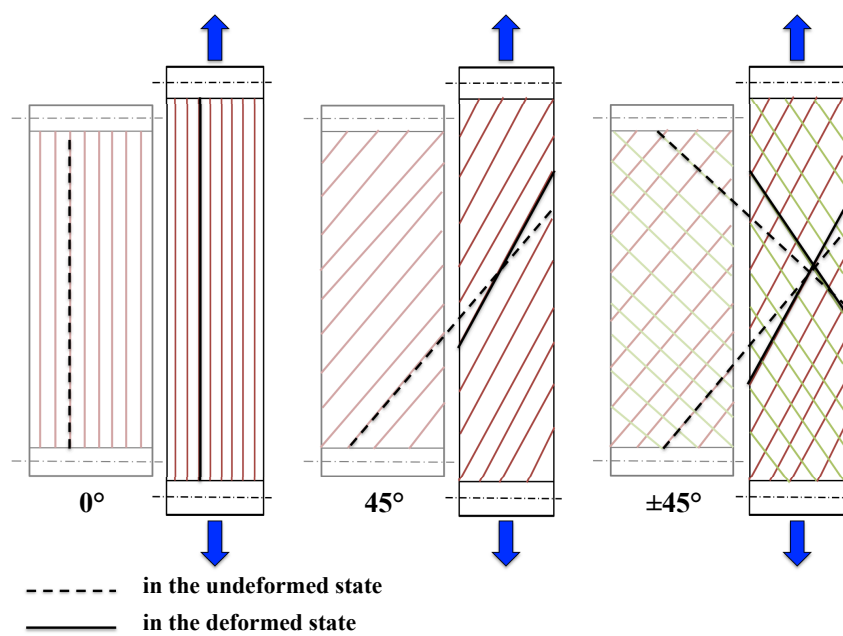


Figure 13: Microstructure reorientation during loading

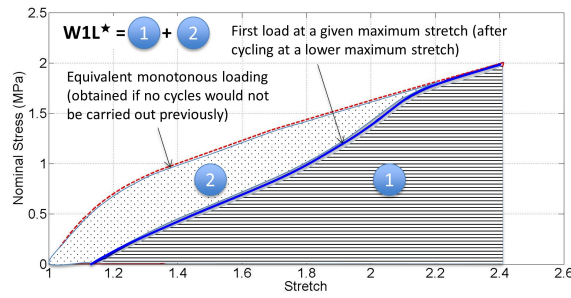


Figure 14: Methodology to calculate W_{1l}^*

A last inelastic phenomenon considered here is the residual strain. It is defined as the strain value when the stress returns to zero at the end of the unloading. Figure 17 depicts its evolution for the three printing configurations. It is clear from these curves that the printing configurations has not a significant effect on the residual strain. Its values were ranged between 8% and 34%.

Figure 18 presents results obtained for the second test, which corresponds to a mechanical cycle at two different loading rates ($\dot{\epsilon} = 50 \text{ mm.min}^{-1}$ and $\dot{\epsilon} = 500 \text{ mm.min}^{-1}$). It should be noted that in the analysis, the softening a.k.a. the Mullins effect is considered as independent of loading rate and is solely function of the strain level. In the case of a TPU for instance, it has been shown experimentally that this assumption was realistic [24]. Also, this assumption has been widely used in modeling of the softening of TPE, see [30], [31], [32] among others. The response for the three deposit configurations 0° , 45° and $\pm 45^\circ$ are presented in Figs 18a, 18b and 18c, respectively. In these figures, the normalized nominal stress ¹ was considered rather than the actual stress in order to assess the time-dependent effects in terms of the drop-off of the nominal stress with respect to the loading rate. All the configurations exhibited a strong effect of

¹normalized with respect to the maximum nominal stress of the high loading rate test

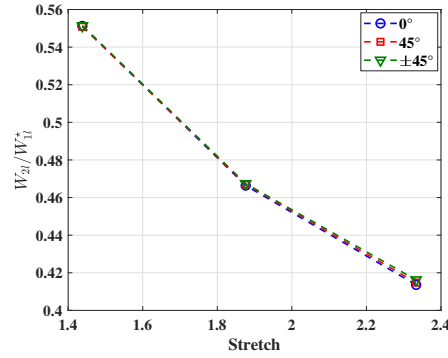


Figure 15: Softening ratio vs stretch for the three configurations

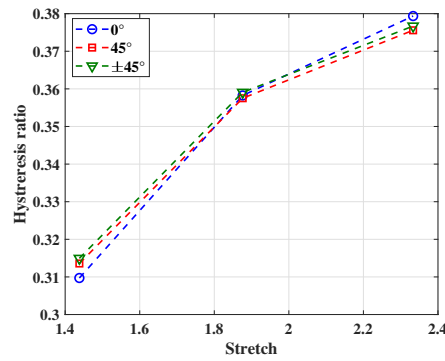


Figure 16: Hysteresis vs stretch for the three configurations

the loading rate on the nominal stress, which is generally assumed to be the consequence of the viscosity. In Fig. 18a corresponding to the 0° configuration, the maximal nominal stress reached for the lowest loading rate was about 91.8% from the one of the highest loading rate. It corresponds to 94.5% for the $\pm 45^\circ$ configuration (see Fig. 18b). It should be noted that failure occurred for the 45° configuration before reaching the maximum strain prescribed for both loading rates. The failure stretch was 2.66 at $\dot{u} = 50 \text{ mm.min}^{-1}$ rate and of 3.43 for the $\dot{u} = 500 \text{ mm.min}^{-1}$. Images of the fractured specimens depicted in Fig. 18b show that the fracture occurred with the same angle, which was equal to the printing angle of 45° . Similar results have been found for other printed polymers using FDM, see [33] for instance.

As a summary, the printing strategy has a slight effect on the mechanical cyclic response; the softening, the hysteresis loop, the permanent set and a strong

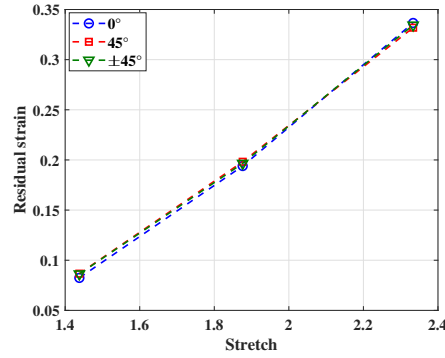


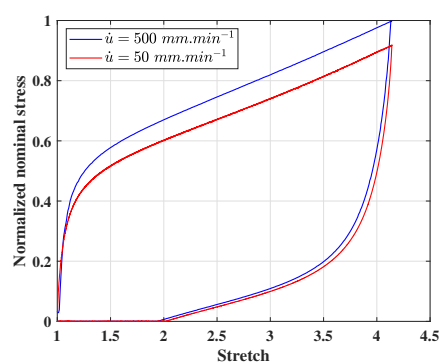
Figure 17: Residual strain vs stretch for the three configurations

effect on the failure. Moreover, the loading rate has a significant effect on the specimens stiffness, which is the manifestation of viscosity. Therefore, a production of intrinsic dissipation is associated with the deformation process, which self-heats the material. As the deposit angle has an effect on viscous effect, the next section investigates the thermal responses according to the deposit angle.

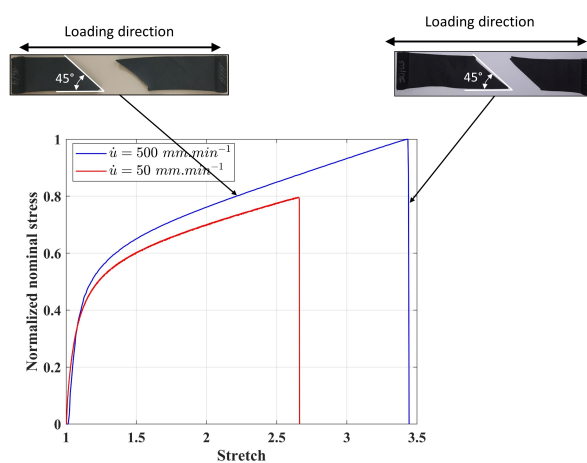
4.2. Thermal response

The thermal response is the consequence of a calorimetric response combined with heat diffusion effects in the case of non-adiabatic effects. The calorimetric response is characterized by the change in the heat power density (expressed in W/m^3) due to two contributions that differ in nature:

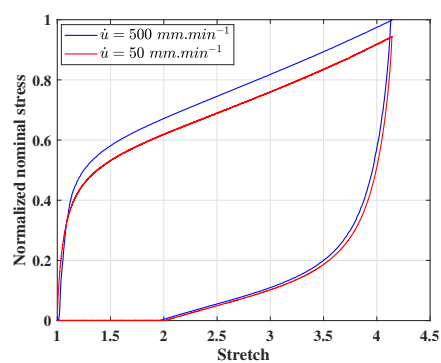
- the intrinsic dissipation, which is a positive quantity corresponding to the heat production due to mechanical irreversibilities during the deformation process, for instance viscosity, stress softening, crack initiation and propagation or more generally damage [34–36]. The intrinsic dissipation leads to a heat production at each mechanical cycle;
- the thermomechanical couplings, which correspond to the couplings between the temperature and state variables and describe reversible deformation processes. Concerning the coupling between temperature and strain, it strongly depends on the origin of the elasticity. In the case of elastomeric materials, this coupling is mainly due to entropic elasticity [37, 38], which leads to an increase in temperature when the strain is increased. Nevertheless, non-entropic effects can be also take place, which leads to the reverse situation [37, 38]. When both occur, a competition is generally observed at the lowest strains and a thermoelastic inversion is observed [39–41].



(a) 0° configuration



(b) 45° configuration



(c) $\pm 45^\circ$ configuration

Figure 18: Normalized nominal stress vs stretch for high and low load rates

245 When intrinsic dissipation is produced under adiabatic test condition, the temperature at the end of the cycle is superior to that at the beginning of the cycle, and the material self-heats. When intrinsic dissipation is produced under non-adiabatic test condition, which is the case in the present study, three situations have to be considered:

- 250 • Situation #1: the heat exchanged with the specimen's outside is superior to the heat produced due to intrinsic dissipation and the temperature at the end of the cycle is inferior to the temperature at the beginning of the cycle;
- 255 • Situation #2 the heat exchanged with the specimen's outside is inferior to the heat produced due to intrinsic dissipation and the temperature at the end of the cycle is superior to the temperature at the beginning of the cycle;
- 260 • Situation #3 the temperature at the end of the cycle is equal to the temperature at the beginning of the cycle, which means that the heat exchanged with the specimen's outside is equal to the heat produced due to intrinsic dissipation. This situation is generally obtained after the first two situations and corresponds to the thermal cycle stabilization.

265 These three situations will be used in the following to analyze the thermal response of the three configurations. Note that the thermal response due to coupling between temperature and strain under non-adiabatic test condition is fully presented and discussed in [42] and [43].

The temperature has been measured at specimens' centre during the mechanical tests. For the first mechanical test performed, the thermal response of the three deposit configurations is reported in Figure 19.

270 Several observations can be firstly made whatever the configuration considered:

- 275 • during the first loading, the temperature variation first dropped before increasing. This phenomenon is classically observed in rubber-like materials and is referred to as the thermoelastic inversion. This inversion in the thermal response is due to the competition between the effects of internal energy variation and entropy variation with respect to the strain level, see for instance [39], [40], [42],
- 280 • a strong self-heating is observed during the first loadings compared to the following ones. This is due to an additional heat production due to the softening effect,²
- the temperature measurement was not correct at the end of each cycle and at the beginning of the next one, as buckling occurs in the zone where

²This heat production can be estimated with a calorimetric approach (see, e.g. [44]).

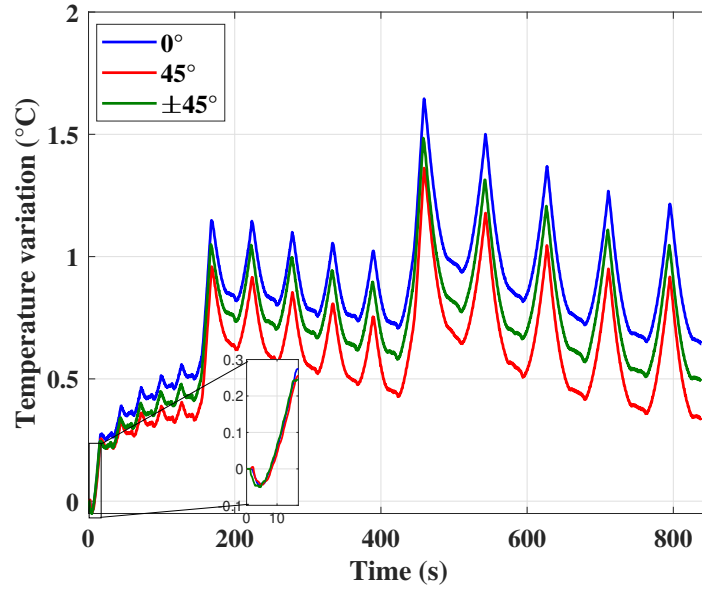
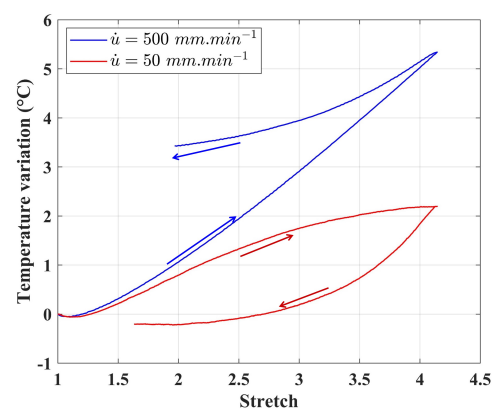


Figure 19: Temperature variation for the three printing configurations

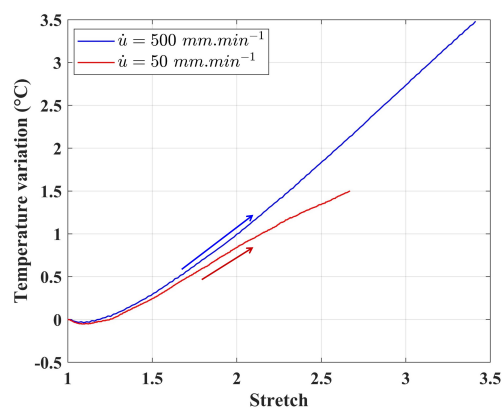
temperature is measured. This out-of-plane effect is due to the permanent set that increases the specimen length when the displacement returns to zero,

- during the first five cycles at a maximum stretch of 1.43, the mean temperature variation increased from one cycle to another. This means that the heat produced during each cycle is higher than that transferred to the specimen outside (Situation #2). This confirms that the mechanical behavior of the printed material has a viscous component, i.e. an intrinsic dissipation due to viscosity is produced at each cycle. It should be noted that thermal stabilization (Situation #3) would have been reached for a higher number of cycles,
- for higher maximum stretches reached (1.87 and 2.33), a strong self-heating is observed after the first loading and the mean temperature variation decreases during the following four cycles (Situation #1). This means that the heat produced during each cycle is lower than that transferred to the specimen outside and is inferior to the heat produced during the first loadings (due to the stress softening).

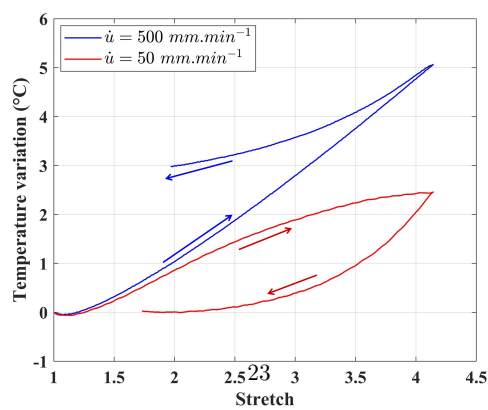
It should be noted that even though the mechanical responses were found very close, the self-heating strongly differs from one configuration to another. The



(a) 0° configuration



(b) 45° configuration



(c) $\pm 45^\circ$ configuration

Figure 20: Temperature variation vs stretch at high and low loading rates

highest self-heating is obtained from the deposit angle of 0° and the lowest for 45° , which confirms the analysis carried out from the tests performed at different loading rates. Therefore, the deposit angle has a significant effect on the viscosity of the specimen. This is an important information for the design of printed parts.

Figure 20 shows the temperature variation measured for the second test, where the three printing configurations were tested at two loading rates. Similarly to the first test, the drop in the material temperature at the beginning of the test was observed for the three configurations, whatever the configuration considered. Also, it can be seen that that temperature variation profile strongly depends on the loading rate.

Under adiabatic conditions, if no intrinsic dissipation is produced, the temperature variation at the end of the cycle is the same as that at the beginning of the cycle and is equal to zero. Under non adiabatic conditions, it is inferior. When intrinsic dissipation occurs under non adiabatic conditions, the temperature variation at the end of the cycle can be superior to the one at the beginning of the cycle if the heat produced is superior to the heat diffused over the cycle. This is typically the case for the higher loading rate applied (see the blue curves for all the configurations).

For same stretch and loading rate, it is possible to define which configuration is the more viscous one. By examining the three diagrams of Fig. 20, it clearly appears that:

- for the 0° configuration, the maximum self-heating was $2.18^\circ C$ for the low loading rate and $5.34^\circ C$ for the high loading rate. The temperature variation at the end of the mechanical loading was $2.9^\circ C$ at this rate,
- for the $\pm 45^\circ$ configuration, the maximum self-heating was about $2.4^\circ C$ for the low loading rate and $5^\circ C$ for the high loading rate with $2.47^\circ C$ remaining temperature at the end of the mechanical loading,
- for the 45° configuration, the self-heating at failure was inferior to the other configurations at the same stretch and loading rate.

As a summary, even though the mechanical responses were found very close from one printing strategy to another, a significant difference was found in terms of self-heating. This difference is due to intrinsic dissipation production induced by viscous effects. It was concluded that the deposit angle of 0° led to a more viscous behavior, the less viscous configuration being the 45° one.

5. Conclusion

In this work, a thermomechanical characterization of 3D-printed soft thermoplastic elastomer obtained by FDM has been carried out. For that purpose, the printer head has been modified. The specimens were obtained by three different printing strategies depending on the angle between the deposit filament

and the tensile direction. Two experiments were carried out with all the studied configurations with two main objectives. The first one is to investigate the thermomechanical behavior of the specimen following the printing strategies. The second one is to assess the influence of the printing strategy on the fracture behavior of the specimens.

The printing strategy was found having a slight effect on the mechanical response; the softening, the hysteresis loop and the permanent set. Moreover, the loading rate had a significant effect on the specimens stiffness, which is the manifestation of viscosity. This has been confirmed by analyzing the stabilized thermal response, which is not affected by the stress softening. It has been found that the deposit angle of 0° led to a more viscous behavior, the less viscous configuration being the 45° one. Furthermore, the thermal responses all exhibit a thermoelastic inversion at low strains. This shows that even though the specimens elasticity is mainly due to entropic effects, non-entropic effects also contribute. The results found in this work present a starting point into the thermomechanical modeling of the printed TPE and a step further into its constitutive equations formulation.

6. Acknowledgements

The authors thank the Cooper Standard and the Elixance companies for supporting this work, Jean-Marc Veillé and Eric Josso for fruitful discussions. The authors thank also the Région Bretagne for financially supporting this work (Région Bretagne grant IMPRIFLEX). SEM images were performed at CMEBA facility (ScanMAT, University of Rennes 1) which received a financial support from the European Union (CPER-FEDER 2007-2014).


References

- [1] S. Bi, E. Chen, S. Gaitanaros, Additive manufacturing and characterization of brittle foams, *Mechanics of Materials* 145 (2020) 103368.
- [2] F. Aghighi, J. Morris, A. V. Amirkhizi, Low-frequency micro-structured mechanical metamaterials, *Mechanics of Materials* 130 (2019) 65–75.
- [3] Y. L. Yap, W. Toh, R. Koneru, K. Lin, K. M. Yeoh, C. M. Lim, J. S. Lee, N. A. Plemping, R. Lin, T. Y. Ng, et al., A non-destructive experimental-cum-numerical methodology for the characterization of 3d-printed materials—polycarbonate-acrylonitrile butadiene styrene (pc-abs), *Mechanics of Materials* 132 (2019) 121–133.
- [4] M. Feygin, S. S. Pak, Laminated object manufacturing apparatus and method, uS Patent 5,876,550 (Mar. 2 1999).
- [5] T. Phillips, S. Fish, J. Beaman, Development of an automated laser control system for improving temperature uniformity and controlling component strength in selective laser sintering, *Additive Manufacturing* 24 (2018) 316–322.

- [6] A. B. Kustas, D. F. Susan, K. L. Johnson, S. R. Whetten, M. A. Rodriguez, D. J. Dagel, J. R. Michael, D. M. Keicher, N. Argibay, Characterization of the fe-co-1.5 v soft ferromagnetic alloy processed by laser engineered net shaping (lens), Additive Manufacturing 21 (2018) 41–52.
- [7] L. E. Murr, S. M. Gaytan, D. A. Ramirez, E. Martinez, J. Hernandez, K. N. Amato, P. W. Shindo, F. R. Medina, R. B. Wicker, Metal fabrication by additive manufacturing using laser and electron beam melting technologies, Journal of Materials Science & Technology 28 (1) (2012) 1–14.
- [8] J. R. C. Dizon, A. H. Espera Jr, Q. Chen, R. C. Advincula, Mechanical characterization of 3d-printed polymers, Additive Manufacturing 20 (2018) 44–67.
- [9] P. Parandoush, D. Lin, A review on additive manufacturing of polymer-fiber composites, Composite Structures 182 (2017) 36–53.
- [10] M. Vaezi, H. Seitz, S. Yang, A review on 3d micro-additive manufacturing technologies, The International Journal of Advanced Manufacturing Technology 67 (5-8) (2013) 1721–1754.
- [11] K. V. Wong, A. Hernandez, A review of additive manufacturing, International scholarly research notices 2012.
- [12] J.-Y. Lee, J. An, C. K. Chua, Fundamentals and applications of 3d printing for novel materials, Applied Materials Today 7 (2017) 120–133.
- [13] R. Liu, Z. Wang, T. Sparks, F. Liou, J. Newkirk, Aerospace applications of laser additive manufacturing, in: Laser additive manufacturing, Elsevier, 2017, pp. 351–371.
- [14] F. P. Melchels, J. Feijen, D. W. Grijpma, A review on stereolithography and its applications in biomedical engineering, Biomaterials 31 (24) (2010) 6121–6130.
- [15] J. L. Ifkovits, J. A. Burdick, Photopolymerizable and degradable biomaterials for tissue engineering applications, Tissue engineering 13 (10) (2007) 2369–2385.
- [16] S. Berretta, R. Davies, Y. Shyng, Y. Wang, O. Ghita, Fused deposition modelling of high temperature polymers: Exploring cnt peek composites, Polymer Testing 63 (2017) 251–262.
- [17] S. Dul, L. Fambri, A. Pegoretti, Fused deposition modelling with abs-graphene nanocomposites, Composites Part A: Applied Science and Manufacturing 85 (2016) 181–191.
- [18] X. Wang, M. Jiang, Z. Zhou, J. Gou, D. Hui, 3d printing of polymer matrix composites: A review and prospective, Composites Part B: Engineering 110 (2017) 442–458.

- 420 [19] C. E. Corcione, F. Gervaso, F. Scalera, S. K. Padmanabhan, M. Madaghiele, F. Montagna, A. Sannino, A. Licciulli, A. Maffezzoli, Highly loaded hydroxyapatite microsphere/pla porous scaffolds obtained by fused deposition modelling, *Ceramics International* 45 (2) (2019) 2803–2810.
- 425 [20] Y. Lee, X. Lu, Y. Hao, S. Yang, R. Uvic, J. R. Evans, C. G. Parini, Rapid prototyping of ceramic millimeterwave metamaterials: Simulations and experiments, *Microwave and Optical Technology Letters* 49 (9) (2007) 2090–2093.
- [21] P. Miranda, A. Pajares, E. Saiz, A. P. Tomsia, F. Guiberteau, Mechanical properties of calcium phosphate scaffolds fabricated by robocasting, *Journal of Biomedical Materials Research Part A: An Official Journal of The Society for Biomaterials, The Japanese Society for Biomaterials, and The Australian Society for Biomaterials and the Korean Society for Biomaterials* 85 (1) (2008) 218–227.
- 435 [22] L. Hirt, A. Reiser, R. Spolenak, T. Zambelli, Additive manufacturing of metal structures at the micrometer scale, *Advanced Materials* 29 (17) (2017) 1604211.
- [23] M. Yoozbashizadeh, P. Yavari, B. Khoshnevis, Novel method for additive manufacturing of metal-matrix composite by thermal decomposition of salts, *Additive Manufacturing* 24 (2018) 173–182.
- 440 [24] A. Lachhab, E. Robin, J.-B. Le Cam, F. Mortier, Y. Tirel, F. Canevet, Thermomechanical analysis of polymeric foams subjected to cyclic loading: Anelasticity, self-heating and strain-induced crystallization, *Polymer* 126 (2017) 19–28.
- 445 [25] L. Mullins, Effect of stretching on the properties of rubber, *Rubber Chemistry and Technology* 21 (2) (1948) 281–300.
- [26] F. Bueche, Molecular basis for the Mullins effect, *Journal of Applied Polymer Science* 4 (10) (1960) 107–114.
- [27] F. Bueche, Mullins effect and rubber-filler interaction, *Journal of Applied Polymer Science* 5 (15) (1961) 271–281.
- 450 [28] G. Marckmann, E. Verron, L. Gornet, G. Chagnon, P. Charrier, P. Fort, A theory of network alteration for the Mullins effect, *Journal of the Mechanics and Physics of Solids* 50 (2002) 2011–2028.
- [29] G. Machado, G. Chagnon, D. Favier, Analysis of the isotropic models of the mullins effect based on filled silicone rubber experimental results, *Mechanics of Materials* 42 (9) (2010) 841–851.
- 455 [30] A. Drozdov, Mullins' effect in thermoplastic elastomers: experiments and modeling, *Mechanics research communications* 36 (4) (2009) 437–443.

- [31] H. Qi, M. Boyce, Constitutive model for stretch-induced softening of the stress–stretch behavior of elastomeric materials, *Journal of the Mechanics and Physics of Solids* 52 (10) (2004) 2187–2205.
- [32] H. J. Qi, M. C. Boyce, Stress–strain behavior of thermoplastic polyurethanes, *Mechanics of materials* 37 (8) (2005) 817–839.
- [33] Y. Song, Y. Li, W. Song, K. Yee, K.-Y. Lee, V. L. Tagarielli, Measurements of the mechanical response of unidirectional 3d-printed pla, *Materials & Design* 123 (2017) 154–164.
- [34] A. Chrysochoos, O. Maisonneuve, G. Martin, H. Caumon, J. O. Chezeau, Plastic and dissipated work and stored energy, *Nuclear Engineering and Design* 114 (1989) 323–333.
- [35] A. Chrysochoos, G. Martin, Tensile test microcalorimetry for thermomechanical behaviour law analysis, *Mater. Sci. Eng. A* 108 (1989) 25–32.
- [36] A. Chrysochoos, V. Huon, F. Jourdan, J. Muracciole, R. Peyroux, B. Watrisse, Use of full-field digital image correlation and infrared thermography measurements for the thermomechanical analysis of material behaviour, *Strain* 46 (2010) 117–130.
- [37] P. J. Flory, A. Ciferri, C. A. J. Hoeve, The thermodynamic analysis of thermoelastic measurements on high elastic materials, *Journal of Polymer Science* 45 (145) (1960) 235–236. doi:10.1002/pol.1960.1204514527. URL <http://dx.doi.org/10.1002/pol.1960.1204514527>
- [38] P. J. Flory, Thermodynamics relation for high elastic materials, *Transactions of the Faraday Society* 57 (1961) 829–838.
- [39] J. P. Joule, On some thermodynamic properties of solids, *Phil Mag* 4th 14 (1857) 227.
- [40] R. L. Anthony, R. H. Caston, E. Guth, Equations of state for naturals and synthetic rubber like materials: unaccelerated natural soft rubber, *Journal of Physical Chemistry* 46 (1942) 826.
- [41] J.-B. Le Cam, Strain-induced crystallization in rubber: A new measurement technique, *Strain* 54 (1) (2018) e12256.
- [42] J. R. Samaca Martinez, J.-B. Le Cam, X. Balandraud, E. Toussaint, J. Cailard, Mechanisms of deformation in crystallizable natural rubber. part 1: thermal characterization, *Polymer* 54 (11) (2013) 2717–2726.
- [43] X. Balandraud, J. B. Le Cam, Some specific features and consequences of the thermal response of rubber under cyclic mechanical loading, *Archive of Applied Mechanics* 84 (6) (2014) 773–788.
- [44] J. R. Samaca Martinez, J.-B. Le Cam, X. Balandraud, E. Toussaint, J. Cailard, New elements on mullins effect: a thermomechanical analysis, *European Polymer Journal* 55 (2014) 98–107.

- 
- Specimens of soft TPE-S were printed by Fused Deposition Modelling
 - Three different deposit angles were considered
 - Thermo-mechanical properties were characterized
 - The printing strategy has not a significant effect on the mechanical response
 - It has a more significant effect on the thermal response, especially the self-heating.

Author contributions

Use this form to specify the contribution of each author of your manuscript. A distinction is made between five types of contributions: Conceived and designed the analysis; Collected the data; Contributed data or analysis tools; Performed the analysis; Wrote the paper.

For each author of your manuscript, please indicate the types of contributions the author has made. An author may have made more than one type of contribution. Optionally, for each contribution type, you may specify the contribution of an author in more detail by providing a one-sentence statement in which the contribution is summarized. In the case of an author who contributed to performing the analysis, the author's contribution for instance could be specified in more detail as 'Performed the computer simulations', 'Performed the statistical analysis', or 'Performed the text mining analysis'.

If an author has made a contribution that is not covered by the five pre-defined contribution types, then please choose 'Other contribution' and provide a one-sentence statement summarizing the author's contribution.

Manuscript title: 3D printing of soft thermoplastic elastomers :effect of the deposit angle on mechanical andthermo-mechanical properties

Author 1: Adel Tayeb

- ☐ **Conceived and designed the analysis**
Specify contribution in more detail (optional; no more than one sentence)
- ☒ **Collected the data**
Specify contribution in more detail (optional; no more than one sentence)
- ☐ **Contributed data or analysis tools**
Specify contribution in more detail (optional; no more than one sentence)
- ☒ **Performed the analysis**
Specify contribution in more detail (optional; no more than one sentence)
- ☒ **Wrote the paper**
Specify contribution in more detail (optional; no more than one sentence)
- ☐ **Other contribution**
Specify contribution in more detail (required; no more than one sentence)

Author 2: Jean-Benoît LeCam

- ☒ **Conceived and designed the analysis**
Specify contribution in more detail (optional; no more than one sentence)
- ☐ **Collected the data**
Specify contribution in more detail (optional; no more than one sentence)
- ☒ **Contributed data or analysis tools**
Specify contribution in more detail (optional; no more than one sentence)
- ☐ **Performed the analysis**
Specify contribution in more detail (optional; no more than one sentence)
- ☒ **Wrote the paper**
Specify contribution in more detail (optional; no more than one sentence)
- ☐ **Other contribution**
Specify contribution in more detail (required; no more than one sentence)

Author 3: Bruno Loez

- ☐ **Conceived and designed the analysis**
Specify contribution in more detail (optional; no more than one sentence)
- ☐ **Collected the data**
Specify contribution in more detail (optional; no more than one sentence)
- ☒ **Contributed data or analysis tools**
Specify contribution in more detail (optional; no more than one sentence)
- ☐ **Performed the analysis**
Specify contribution in more detail (optional; no more than one sentence)
- ☐ **Wrote the paper**
Specify contribution in more detail (optional; no more than one sentence)
- ☒ **Other contribution**
Provided 3D printed samples following several printing strategies

Conflict of interest statements

Manuscript title: 3D printing of soft thermoplastic elastomers: effect of the deposit angle on mechanical and thermo-mechanical properties.

The authors whose names are listed immediately below certify that they have NO affiliations with or involvement in any organization or entity with any financial interest (such as honoraria; educational grants; participation in speakers' bureaus; membership, employment, consultancies, stock ownership, or other equity interest; and expert testimony or patent-licensing arrangements), or non-financial interest (such as personal or professional relationships, affiliations, knowledge or beliefs) in the subject matter or materials discussed in this manuscript.

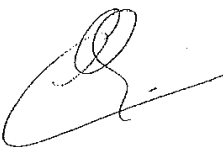
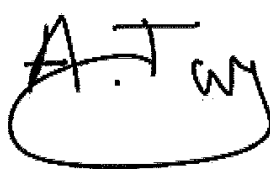
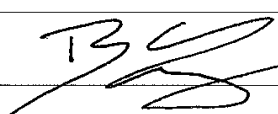
Author names:

Adel Tayeb

Jean-Benoît Le Cam

Bruno Loez

This statement is signed by all the authors to indicate agreement that the above information is true and correct

Author's name	Author's signature	Date
Jean-Benoît Le Cam		08/28/2020
Adel Tayeb		08/28/2020
Bruno Loez		08/28/2020